

Bandstructure Effects in Multiwall Carbon Nanotubes

Bernhard Stojetz and Christoph Strunk

Institute of Experimental and Applied Physics, University of Regensburg, 93040 Regensburg, Germany

Csilla Miko and Laszlo Forró

Institute of Physics of Complex Matter, FBS Swiss Federal Institute of Technology (EPFL), CH-1015 Lausanne, Switzerland

(Dated: October 31, 2004)

We report conductance measurements on multiwall carbon nanotubes in a perpendicular magnetic field. A gate electrode with large capacitance is used to considerably vary the nanotube Fermi level. This enables us to search for signatures of the unique electronic band structure of the nanotubes in the regime of diffusive quantum transport. We find an unusual quenching of the magnetoconductance and the zero bias anomaly in the differential conductance at certain gate voltages, which can be linked to the onset of quasi-one-dimensional subbands.

PACS numbers:

Quantum transport in multiwall carbon nanotubes has been intensely studied in recent years [1, 2]. Despite some indications of ballistic transport even at room temperature [3, 4], the majority of experiments revealed typical signatures of diffusive quantum transport in a magnetic field B such as weak localization (WL), universal conductance fluctuations (UCF) and the $h/2e$ -periodic Altshuler-Aronov-Spivak (AAS) oscillations [2, 5, 6, 7]. These phenomena are caused by the Aharonov-Bohm phase, either by coherent backscattering of pairs of time-reversed diffusion paths (WL and AAS) or by interference of different paths (UCF). In addition, zero bias anomalies caused by electron-electron interactions in the differential conductance have been observed [8]. In those experiments, the multiwall tubes seemed to behave as ordinary metallic quantum wires. On the other hand, bandstructure calculations for singlewall nanotubes predict strictly one-dimensional transport channels, which give rise to van Hove singularities in the density of states [9]. Experimental evidence for this has been obtained mainly by electron tunneling spectroscopy on single wall nanotubes [10]. In this picture of strictly one-dimensional transport a quasiclassical trajectory cannot enclose magnetic flux and no low-field magnetoconductance is expected. Hence, the question arises how the specific band structure is reflected in the conductance as well as in its quantum corrections and how those on first glance contradictory approaches can be merged into a consistent picture of electronic transport.

In this experiment, we use a strongly coupled gate, which is efficient enough to shift the Fermi level through several quasi-one-dimensional subbands. At certain gate voltages, which can be associated with the bottoms of the subbands, we observe a strong suppression of both the magnetoconductance and the differential conductance.

The samples were produced on top of thermally oxidized Silicon wafers. First, Aluminium strips of $10\ \mu\text{m}$ width and $40\ \text{nm}$ thickness were evaporated. Exposure to air provides an insulating native oxide layer of a few nm thickness. These strips serve as a backgate for the individual nanotubes, which are deposited from a chlo-

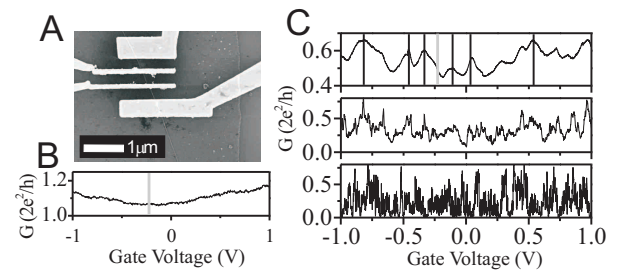


FIG. 1: (A) SEM image of a typical sample: individual multiwall nanotubes are deposited on a prestructured Al gate electrode and contacted by four Au fingers, which are deposited on top of the tube. The electrode spacing is $300\ \text{nm}$. For the measurements, only the two inner electrodes are used. (B) Room temperature conductance of sample A as a function of gate voltage in units of the conductance quantum $2e^2/h$. The estimated position of the charge neutrality point corresponds to the minimum of conductance and is indicated by a grey line. (C) Same as in Fig. 1B, but for $10\ \text{K}$, $1\ \text{K}$ and $30\ \text{mK}$ (top to bottom). For the $10\ \text{K}$ curve, both the positions of the charge neutrality point (grey line) and the regions of quenched magnetoconductance (black lines) as observed in Fig. 2 are indicated.

reform suspension in the next step. Electric contacts are defined by electron beam lithography. After application of an oxygen plasma, $80\ \text{nm}$ of Gold are deposited. In this way we achieve typical resistances between $10\ \text{k}\Omega$ and $30\ \text{k}\Omega$ at $4.2\ \text{K}$. The samples were operated by a low frequency ac bias voltage and application of a dc gate voltage U_{Gate} to the Aluminium layer. Up to gate voltages of $3\ \text{V}$ no leakage current between the gate and the tube was observed ($I_{\text{Leak}} < 100\ \text{fA}$). Typical breakdown voltages of the gate oxide were $3\text{-}4\ \text{V}$. Two-terminal resistance measurements were carried out for two samples, A and B. The lengths of the samples are $5\ \mu\text{m}$ and $2\ \mu\text{m}$ and their diameters are $19\ \text{nm}$ and $14\ \text{nm}$, respectively. A scanning electron micrograph of a typical sample is presented in Fig. 1A.

In order to characterize the dependence of the conductance of sample A on U_{Gate} , a small ac bias voltage of

$2 \mu\text{V} \ll k_{\text{B}}T$ was applied and the current was measured at several temperatures T (Fig. 1B,C). Fig. 1B shows the conductance G as a function of gate voltage at 300 K. The corresponding curves for 10 K, 1 K and 30 mK are presented in Fig. 1C. The conductance at room temperature exhibits a shallow minimum located at $U_{\text{Gate}} \approx -0.2$ V. When the Fermi level is tuned away from the charge neutrality point, more and more subbands can contribute to the transport and an increase of the conductance is expected. Thus we attribute the position of the conductance minimum to the charge neutrality point, where bands with positive energy are unoccupied while those with negative energies are completely filled [11]. This reveals the high efficiency of the gate as well as an intrinsic n -doping of the tube. The location of the minimum varied from sample to sample. We observed p - as well as n -doping at $U_{\text{Gate}} = 0$ V in several samples. The $G(U_{\text{Gate}})$ curves in Fig. 1C show an increasing amplitude of the conductance fluctuations as the temperature is lowered, while the average conductance decreases. This can be interpreted as a gradual transition from a coexistence of band structure effects, UCFs and charging effects at 10 K and 1 K to the dominance of Coulomb blockade at 30 mK. In contrast to experiments on clean single wall nanotubes, no periodic Coulomb oscillations are found. Instead, irregular peaks in conductance occur. It is likely that disorder induces a nonuniform series of strongly coupled quantum dots and that transport is governed by higher order tunneling processes [12].

Next, conductance traces $G(U_{\text{Gate}})$ were recorded at several temperatures and in magnetic fields perpendicular to the tube axis. The result at a temperature of 10 K is displayed as a color plot in Fig. 2A. We have checked for several gate voltages that $G(B)$ is symmetric with respect to magnetic field reversal as required in a two point configuration (not shown). In addition, most of the curves show a conductance minimum at zero magnetic field. A closer look at the data reveals that both the amplitude and the width of the conductance dip vary strongly with gate voltage. In order to make this variation more visible, we subtracted the curve at zero magnetic field (see Fig. 1C) from all gate traces at finite fields. The deviation from the zero-field conductance is presented as a color plot in Fig. 2B. The most striking observation is that the magnetoconductance (MC) disappears at certain gate voltages U^* , as indicated by arrows. These voltages U^* are grouped symmetrically around the conductance minimum at $U_{\text{Gate}} \approx -0.2$ V in Fig. 1B, which we have assigned to the charge neutrality point. The position of the latter, as well as the gate voltages of MC quenches have been indicated also in the linear response conductance curve (Fig 1C) by red and black vertical lines, respectively. The latter always coincide with conductance maxima. These observations lead us to the conjecture that the quenched MC may occur at the onset of subbands of the outermost nanotube shell, which is believed to carry the major part of the current at low temperatures [7].

To confirm this idea, we applied a simple bandstructure model. The black line in Fig. 3A shows the density of states of a single wall (140,140) armchair nanotube, which matches to the diameter of sample A (19 nm). Typical van Hove singularities arise at the energies, where the subband bottoms are located [9]. By integration over energy one obtains the number ΔN of excess electrons on the tube, plotted as a red line in Fig. 3A. In this way, we can determine the number ΔN^* of electrons at the onset of the nanotube subbands. If we assume as usual a capacitive coupling between the gate and the tube, ΔN can be converted into a gate voltage via $CU_{\text{Gate}} = e\Delta N$. In Fig. 3B the measured gate voltages U^* of quenched MC are plotted versus the calculated ΔN^* for both samples. Both data sets fit very well into straight lines, which demonstrates that most of the positions U^* of the quenched MC agree very well with the expected subband onsets. In addition, the gate capacitances C are provided by the slope of U^* vs. ΔN^* . The capacitances per length are nearly identical, i.e. 120 aF/ μm and 129 aF/ μm for samples A and B, respectively. These values agree within a factor of 2 with simple geometrical estimates of C , indicating the consistency of the interpretation. From the capacitance C and the calculated dependence of the number of electrons N on energy one can convert the gate voltage into an equivalent Fermi energy. This energy scale is shown in Fig. 2F.

The typical dip in the MC at $B = 0$ in Fig. 2A has been observed earlier and can be explained in terms of weak localization in absence of spin-orbit scattering [2, 6, 13]. The weak localization correction ΔG_{WL} to conductance provides information on the phase coherence length L_{φ} of the electrons. With W being the measured diameter and $L = 300$ nm the electrode spacing of the nanotube, ΔG_{WL} is given in the quasi-one-dimensional case ($L_{\varphi} > W$) by $\Delta G_{\text{WL}} = -(e^2/\pi\hbar L) \cdot (L_{\varphi}^{-2} + W^2/3\ell_m^4)^{-1/2}$, where $\ell_m = (\hbar/eB)^{1/2}$ is the magnetic length. In Fig. 2B each row displays a dip around zero magnetic field, where both the amplitude and the width of the dip vary strongly with gate voltage. We have used the weak localization expression above to fit the low field MC with L_{φ} and $G(B = 0)$ as free parameters. The conductance ΔG_{WL} as calculated using the fit parameters is plotted in Fig. 2C. We find that conductance traces are reproduced very well by the fit for fields up to 2 T. For higher fields, deviations occur, most probably due to residual universal conductance fluctuations. In this way we obtain an energy dependent phase coherence length $L_{\varphi}(E_{\text{F}})$, which is plotted in Fig. 2D. L_{φ} varies from 20 to 60 nm and displays pronounced minima which correspond to the regions of nearly flat MC in Fig. 2B. From the preceding discussion, we can say that weak localization seems to be suppressed at the onset of nanotube subbands.

In order to confirm the validity of our interpretation in terms of weak localization, we have studied the temperature dependence of the phase coherence length. As the dominating dephasing mechanism, quasielastic electron-electron scattering has been identified [2, 6, 14]. De-

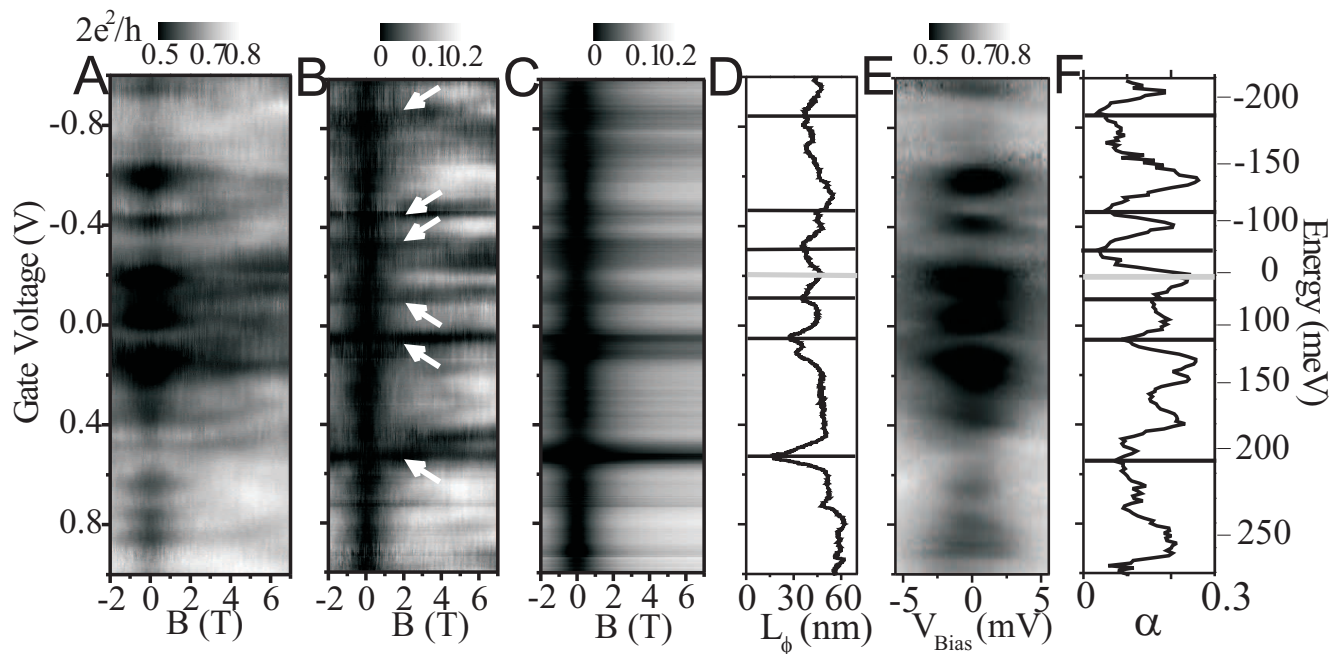


FIG. 2: (A) Grey scaled conductance G of sample A as a function of gate voltage U and perpendicular magnetic field at a temperature of 10 K. (B) Deviation of G from the zero-field conductance $G(U, B) - G(U, 0)$. White arrows indicate the regions of quenched magnetoconductance. (C) Reproduction of the magnetoconductance by 1D weak localization fits. The parameters L_ϕ and $G(B = 0)$ are used as obtained by fitting the data on Fig. 2A. (D) Phase coherence length L_ϕ vs. gate voltage as obtained from the fit. The positions of the charge neutrality point (grey line) and the regions of quenched magnetoconductance (black lines) are indicated. (E) Differential conductance of sample A as a function of gate voltage and dc bias voltage V_{Bias} at $T=10$ K. (F) Exponent α vs. gate voltage as obtained from fitting a power law V^α to the differential conductance in the range $eV \gg k_B T$. Right: scale conversion of the gate voltage into a (nonlinear) energy scale using the gate capacitance as obtained from Fig. 3B.

phasing by electron-phonon scattering is negligible since the corresponding mean free path exceeds $1 \mu\text{m}$ even at 300 K [15, 16]. The theory by Altshuler, Aronov and Khmel'nitzky [17] predicts $L_\phi = (GDL\hbar^2/2e^2k_B T)^{1/3}$, where G is the conductance, D is the diffusion constant, L is the length of the tube. The dominance of electron-electron-scattering can be confirmed by studying the temperature dependence of L_ϕ . Therefore, the MC measurements have been repeated for temperatures ranging from 1 K to 60 K. In order to eliminate the contribution of the universal conductance fluctuations, the MC curves have been averaged over all gate voltages. The result is plotted in Fig. 4A. For the comparison of the curves with theory, one has to bear in mind that the average runs also on curves with suppressed MC. Hence, for the fit an averaged weak localization contribution of the form $\Delta G_{\text{WL}}^* = A \cdot \Delta G_{\text{WL}}$ with a scaling factor $0 < A < 1$ has been taken into account. The fitted curves are included in Fig. 4A. They match the data very well, up to magnetic fields of 7 T. In Fig. 4B the resulting $L_\phi(T)$ are presented. The contribution of the universal conductance fluctuations is completely suppressed by ensemble averaging. The temperature dependence matches a power law with exponent -0.31, which is close to the theoretical prediction of -1/3.

Another quantum correction to the conductance is in-

duced by the electron-electron-interaction and reduces the density of states near the Fermi energy [18]. This leads to zero bias anomalies in the differential conductance dI/dV [8], from which information on the strength of the electron-electron-interaction can be extracted. In the case of tunneling into an interacting electron system with an ohmic environment, the differential conductance dI/dV is given by a power law, i.e. $dI/dV \propto V^\alpha$ for $eV \gg k_B T$, where the exponent α depends both on the interaction strength and the sample geometry [19]. In order to obtain complementary information, we have examined the dependence of the ZBA on the gate voltage U_{Gate} . The differential conductance has been measured as a function of U_{Gate} and V_{Bias} . The result is presented in Fig. 2E. For each gate voltage, the conductance shows a dip at zero bias. The zero bias anomaly has a strongly varying width with gate voltage and nearly vanishes at the same gate voltages $U_{\text{Gate}} = U^*$ as the magnetoconductance. For each value of the gate voltage, a power law fit for the bias voltage dependence of the differential conductance has been performed. The resulting exponent $\alpha(U_{\text{Gate}})$ is plotted in Fig. 2F. α varies between 0.03 and 0.3 and shows pronounced minima at the gate voltages U^* .

We thus observe experimentally a strong correlation between the single particle interference effects (expressed by

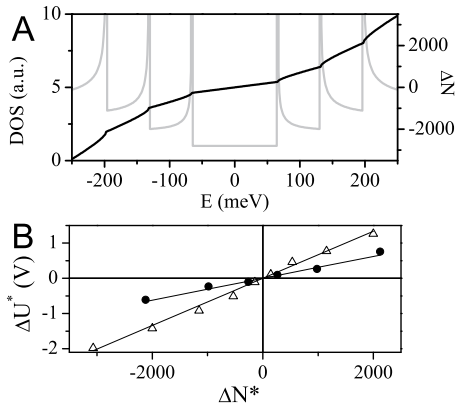


FIG. 3: (A) Calculated π -orbital density of states (DOS) for a (140,140) armchair nanotube of diameter of 19 nm (grey) as a function of energy. Number of excess electrons $N(E)$ (black) as obtained from the integration of the DOS from 0 to E . The subband spacing for this diameter is 66 meV. (B) Measured gate voltage values U^* of nanotube subband onsets vs. calculated numbers of electrons ΔN^* at subband onsets for sample A (circles, diameter 19 nm) and B (triangles, diameter 14 nm). The lines correspond to linear fits of the data. The slopes of the lines correspond to gate capacitances per length of 120 aF/ μ m and 129 aF/ μ m for sample A and B, respectively.

L_φ) and the interaction effects (expressed by α). Both are strongly reduced at certain positions of the Fermi level, which match well the positions of the van Hove singularities estimated from simple bandstructure models. What is the effect of the bandstructure? Numerical calculations by Triozon et al. [20] indicate that the diffusion coefficient D is not a constant as a function of E_F , but displays pronounced minima at the onset of new subbands. At these points strong scattering occurs, resulting from the opening of a highly efficient scattering channel. This has a direct effect on $L_\varphi = \sqrt{D(E_F)\tau_\varphi}$. Of course, τ_φ may also be affected.

Can the energy dependence of $D(E_F)$ also explain the suppression of the interaction effects? This question has already been raised by Kanda et al. [21], who also observed a pronounced gate modulation of α . For weak electron-electron-interaction the theory of Ref. [18] predicts $\alpha \propto 1/\ell_{el}$, where ℓ_{el} is the elastic mean free path. This is definitely incompatible with the observed suppression of α at Fermi levels where diffusion is slow. The observed strong modulations of L_φ and α are accompanied by a rather weak modulation of the zero bias conductance at 10 K (see Fig. 1B). One may thus ask, whether the assumption of weak interactions is valid. Taking the simple Drude formula $\sigma = e^2 N(E_F)D(E_F)$ as an orientation, this can be explained by a partial compensation of the variation of N and D with E_F . However, a quantitative

explanation of the observed interplay between bandstructure effects and quantum corrections to the conductance

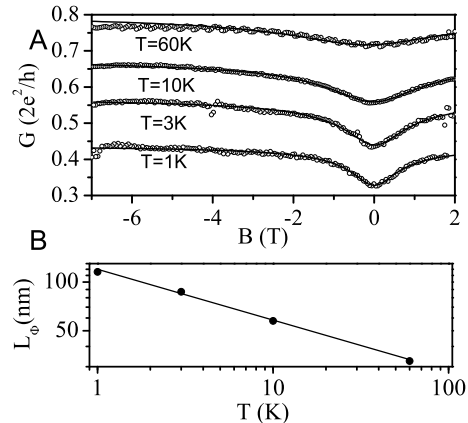


FIG. 4: (A) Averaged magnetoconductance of sample A (circles) at temperatures of 60 K, 10 K, 3 K and 1 K (top to bottom) and fits of 1D weak localization behavior (lines). (B) Double-logarithmic plot of the temperature dependence of the phase coherence length L_φ as obtained from the weak localization fit (black dots). The line corresponds to a power law fit with an exponent -0.31.

requires a realistic model calculation for a thick, e.g., (140,140) nanotube including disorder and interaction effects. The simple model of strictly one-dimensional conductance channels is obviously incompatible with the observed weak-localization-like magnetoconductance close to the charge neutrality point. The disorder must be strong enough to mix the channels without completely smearing the density of states.

In conclusion, our electronic transport measurements on multiwall carbon nanotubes reveal an interplay of bandstructure effects originating from the geometry of the tube and quantum interference induced by disorder. The results demonstrate the necessity of a systematic theoretical approach which can account both for disorder and geometrical effects on the same level.

Acknowledgments

We have benefitted from inspiring discussions with A. Bachtold, V. Bouchiat, G. Cuniberti, H. Grabert, M. Grifoni, K. Richter, S. Roche, R. Schäfer, C. Schönberger and F. Triozon. Funding by the Deutsche Forschungsgemeinschaft within the Graduiertenkolleg 638 is acknowledged. The work in Lausanne was supported by the Swiss National Science Foundation.

-
- [1] C. Dekker, *Physics Today* **52** 22 (1999).
 - [2] C. Schönenberger *et al.*, *Appl. Phys. A* **69** 283 (1999).
 - [3] S. Frank *et al.*, *Science* **280** 1744 (1998).
 - [4] A. Urbina *et al.*, *Phys. Rev. Lett.* **90**, 106603 (2003).
 - [5] L. Langer *et al.*, *Phys. Rev. Lett.* **76**, 479 (1996).
 - [6] K. Liu *et al.*, *Phys. Rev. B* **63** 161404 (2001).
 - [7] A. Bachtold *et al.*, *Nature* **397**, 673 (1999).
 - [8] A. Bachtold *et al.*, *Phys. Rev. Lett.* **87**, 166801 (2001).
 - [9] R. Saito *et al.*, *J. Appl. Phys.* **73** 494 (1993).
 - [10] S. J. Tans *et al.*, *Nature* **393** 49 (1998).
 - [11] M. Krüger *et al.*, *New J. Phys* **5** 138.1 (2003).
 - [12] P. L. McEuen *et al.*, *Phys. Rev. Lett.* **83**, 5098 (1999).
 - [13] R. Tarkianinen *et al.*, *Phys. Rev. B* **64**, 195412 (2001).
 - [14] B. Stojetz *et al.*, *New J. Phys* **6** 27 (2004).
 - [15] J.-Y. Park *et al.*, *Nano Lett.* **4**, 517 (2004).
 - [16] A. Javey *et al.*, *Phys. Rev. Lett.* **92**, 106804 (2004).
 - [17] B. L. Altshuler, A. G. Aronov and D. Khmelnitzky, *Solid State Comm.* **39**, 619 (1981).
 - [18] R. Egger and A. O. Gogolin, *Phys. Rev. Lett.* **87**, 066401 (2001).
 - [19] C. L. Kane and M. P. W. Fisher, *Phys. Rev. B* **46**, 15233 (1992).
 - [20] F. Triozon *et al.*, *Phys. Rev. B* **69**, 121410 (2004).
 - [21] A. Kanda *et al.*, *Phys. Rev. Lett.* **92**, 026801 (2004).